New Journal of Physics
The open access journal at the forefront of physics

Deutsche Physikalische Gesellschaft DPG IOP Institute of Physics

Pumping fluid by magnetic surface stress

To cite this article: Robert Krauß *et al* 2006 *New J. Phys.* **8** 18

New Journal of Physics
The open–access journal for physics

Pumping fluid by magnetic surface stress

Robert Krauß[1], Mario Liu[2], Bert Reimann[1], Reinhard Richter[1] and Ingo Rehberg[1]

[1] Experimentalphysik V, Universität Bayreuth, D-95440 Bayreuth, Germany
[2] Institut für Theoretische Physik, Universität Tübingen, D-72076 Tübingen, Germany
E-mail: robert.krauss@uni-bayreuth.de

New Journal of Physics **8** (2006) 18
Received 3 November 2005
Published 31 January 2006
Online at http://www.njp.org/
doi:10.1088/1367-2630/8/1/018

Abstract. A magnetic field rotating on the free surface of a ferrofluid layer is shown to induce considerable fluid motion towards the direction the field is rolling. The measured flow velocity (i) increases with the square of the magnetic field amplitude, (ii) is proportional to the thickness of the fluid layer and (iii) has a maximum at a fluid specific frequency. The pumping speed can be estimated with a two-dimensional flow model. We compare the pumping performance of a magnetic fluid based on magnetite with the performance of a novel fluid based on cobalt.

Contents

1. Introduction

Polarizable fluids can show a macroscopic reaction to external electric or magnetic fields. While for most fluids the influence of a magnetic field is fairly weak, colloidal suspensions of magnetic particles—so-called ferrofluids—do show a strong response particularly to static magnetic fields [1, 2]. If these fields are time dependent, a rich variety of phenomena occurs. To give an example, it has been shown, in experiment and theory, that *alternating* magnetic fields can increase or decrease the viscosity in a capillary flow [3, 4]. However, there the decrease of the viscosity was only about 1% which is far too small to excite a spontaneous flow, driven solely by magnetic forces. On the other hand, the driving of a macroscopic flow by means of an external *rotating* magnetic field has been demonstrated to be possible: a field rotating in the plane spins up a rotational flow in an open beaker [5, 6]. However, due to the unsuitable geometry, only a tiny part of the fluid is here contributing to the flow. The curvature of the meniscus plays a decisive role [7], and a quantitative description has remained for long unsatisfactory.

The driving force behind the fluid motion is the tangential stress which has its origin in the spatial inhomogeneity of $\boldsymbol{M} \times \boldsymbol{H}$ [8]–[10]. The inhomogeneity of the magnetization is maximal at the surface of the fluid, where it decays in a step-like manner to the vacuum value. Thus, for an effective driving, it is most important that this drastic decay is exploited at the whole free surface of the fluid. For this purpose, the rotation vector has to be perpendicular to the normal vector of the surface.

One possible realization of this condition is a system of coaxial cylinders filled with ferrofluid [11]–[14]. The outer cylinder is fixed, and the inner one is freely suspended, in this way serving as a vertical realization of a free surface. In [14] this geometry has been utilized to measure the tangential stress acting on the inner cylinder and to perform a first quantitative comparison of theory and experiment.

In this paper, we realize an optimal driving of the fluid with a different geometry, suitable for the transport of fluid in open channels [15, 16]. It is attractive, because it allows for a very fine tuning both of the speed and of the direction of the flow even in microscopic channels. To facilitate a quantitative comparison of the measured flow velocities with its theoretical estimation, we have chosen a circular duct, as shown in figure 1. The experiments described in this paper were carried out with two different kinds of ferrofluids. We compare the flow of a magnetite-based fluid with a novel magnetic fluid synthesized from cobalt.

2. Experimental setup

A circular Macrolon® duct with a mean diameter d of 100 mm and a square cross-section of 5 mm × 5 mm is filled brimful with magnetic fluid. For additional measurements, cross-sections of 2.5 mm × 2.5 mm and 10 mm × 10 mm were used. The orientation of the two coils producing the rotating magnetic field is also indicated in figure 1(a): one coil is wrapped around this circular channel and provides a magnetic field in azimuthal direction, and the outer coil produces the vertical component of the field. Both coils are driven with an ac-current with a phase difference of 90°, thus producing a rotating field on the free surface of the fluid within the duct.

For the experiments, two kinds of magnetic fluids have been used: a conventional fluid, based on magnetite, was synthesized via the Khallafalla reaction. Its viscosity has been determined by a low shear rheometer (Contraves LS40) to 10.0 m Pa s at room temperature. A novel fluid

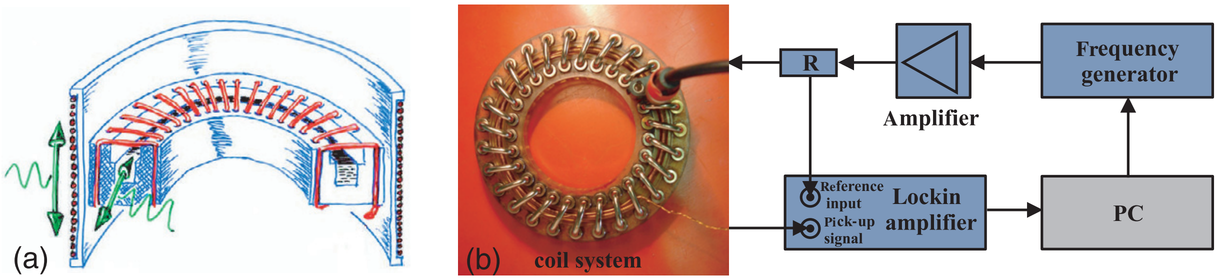

Figure 1. (a) Experimental setup for the investigation of the magnetic liquid flow. The arrows indicate the direction of the oscillating magnetic fields provided by the coils. (b) Schematic setup for the susceptibility measurements.

synthesized from air stable colloidal cobalt particles [17, 18] was investigated because of its large complex susceptibility. Its viscosity has been determined to be 5.4 m Pa s. Both fluids are stabilized by oleic acid in kerosene.

The characterization of the complex magnetic susceptibility of the fluids in the duct is of primary importance for the pumping of the fluid, as discussed in this paper. To measure this quantity, a pick-up coil was immersed in the liquid. The complete schematic setup is displayed in figure 1(b). Here the toroidal field-coil is composed from removable jumpers, which facilitates a proper cleaning of the circular duct. The field-coil is connected via a high precision resistance to a highly linear power amplifier (Rotel RB-1090), which obtains its sinusoidal input from a function generator (Fluke PM 5138A). The voltage drop at the resistance serves as reference input for the lockin amplifier (Stanford Research Systems SR 830 DSP). Its other input is connected to the pick-up coil. The arrangement is calibration free, because the magnetization is determined from the difference of the signal detected by the pick-up coil in the empty and the filled channel. Via control of a PC the magnetization has been measured as a function of frequency of the external oscillating azimuthal magnetic field. The results are presented in figure 2. The measured susceptibilities of the magnetite-based fluid are surmounted by one of the cobalt-based fluid. In particular, the imaginary parts differ in an order of magnitude from each other and their maxima are at about 10 and 1 kHz, respectively. These deviations are due to the different composition of the ferrofluid samples [19]. Notably, the large crystal anisotropy of the Co particles is responsible for their large imaginary part of the susceptibility. A large imaginary part is essential for the pumping action described in this paper.

3. Experimental results

A rotating field produced by the coils leads to a motion of the fluid in azimuthal direction of the channel, as reported in a recent letter [20]. Its velocity is on the order of mm s^{-1} and can thus be determined by visual inspection of tracer particles swimming on its surface. The next observation is also a qualitative one: when changing the phase difference between the ac fields from $+90^\circ$ to -90°, the flow changes its sign. The flow direction is such that the vorticity of the flow field is locally parallel to the rotation vector of the magnetic field, i.e. the fluid flows towards the direction the field is rolling. The working pump and the flow reversion can be viewed in the

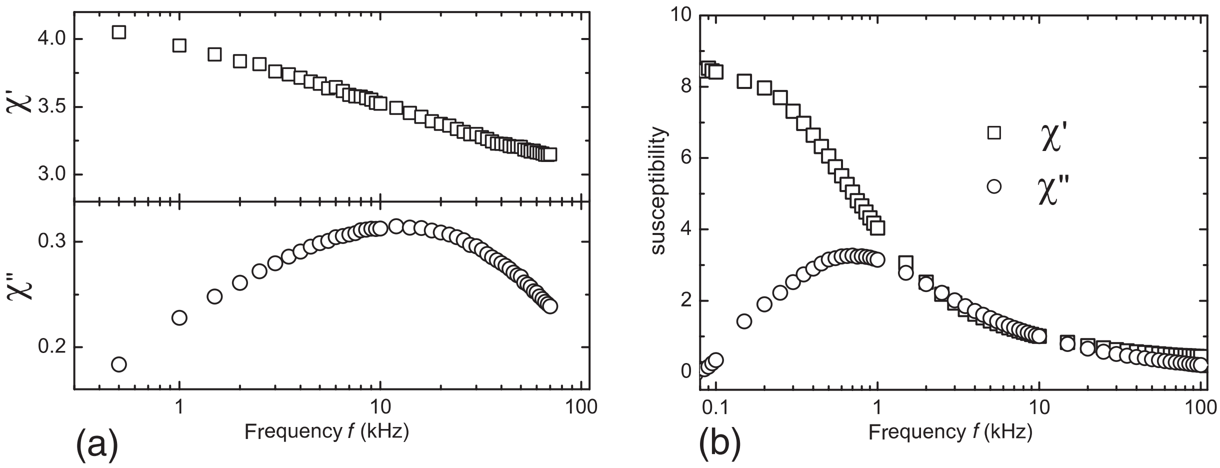

Figure 2. The magnetic susceptibility of the magnetite liquid (a) and the cobalt-based liquid (b) as a function of the frequency of the external alternating magnetic field. Here the real and imaginary parts are denoted by squares and circles, respectively.

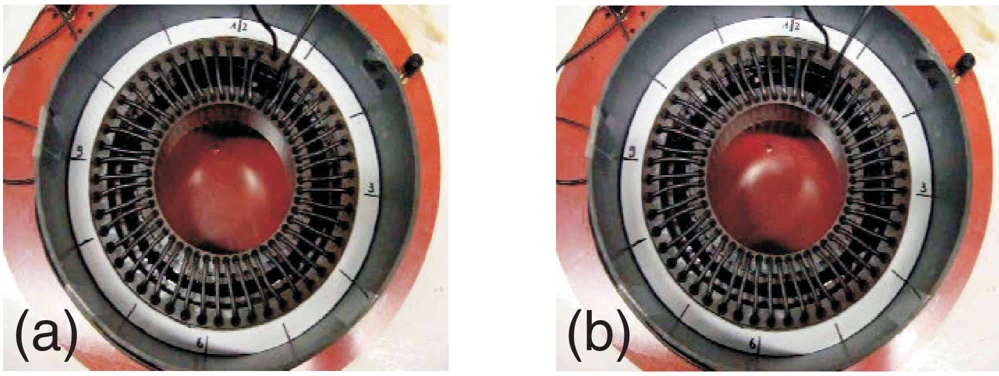

Figure 3. Top view of the duct and surrounding coils. (a) Clockwise (movie 1) and (b) counterclockwise (movie 2) flow of the fluid are realized.

movies connected with figure 3. For better visualization, the movies were recorded by using a fairly large synthetic tracer particle.

For quantitative measurements, it is necessary to use particles which are small compared to the channel width. Best results have been obtained with dandruff, with a diameter of about 1 mm. The velocity is determined by taking the time a particle needs to travel a few centimetres. The size dependence of these measurements is taken into account by using the numerically calculated—roughly parabolic—velocity profiles, and by assuming that a floating particle represents the mean speed with respect to its diameter. Results obtained for a fixed frequency are presented in figure 4, where the maximal flow velocity within the channel is shown as a function of the amplitude G_0 of the driving external magnetic field. For both fluid samples, the velocity increases proportional to G_0^2, as demonstrated by the solid line, a parabola. Here we follow the nomenclature of [21], where the external magnetic far field is marked by $\boldsymbol{G}$ and the local one by $\boldsymbol{H}$.

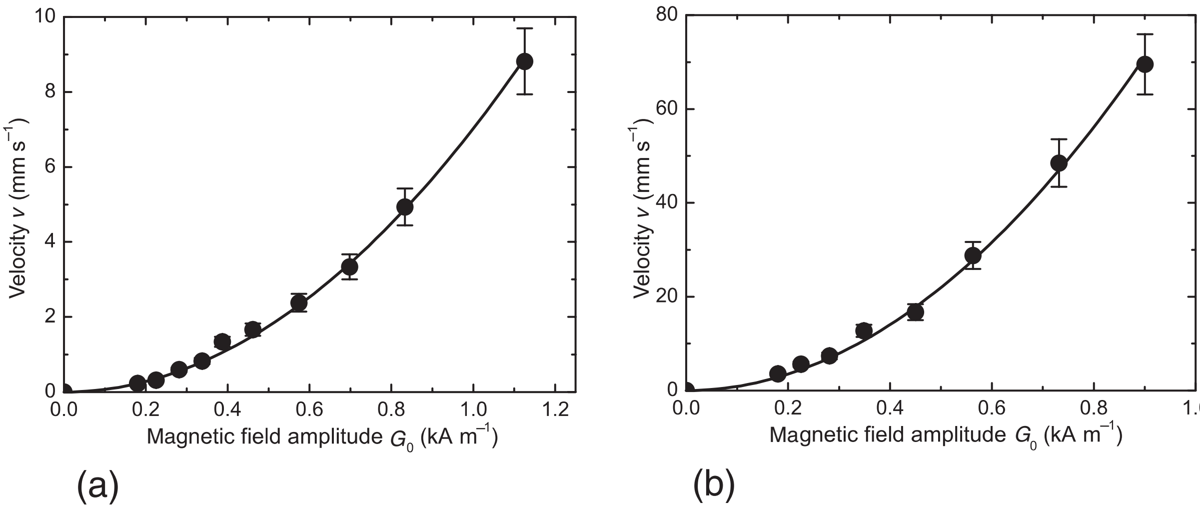

Figure 4. Maximal velocity measured as a function of the field amplitude: (a) magnetite fluid sample at a fixed frequency of 10 kHz, (b) cobalt fluid sample at a fixed frequency of 1 kHz.

Having demonstrated this quadratic dependence of the velocity on the magnetic field, the first approach to collapse data obtained at different fields is to introduce a reduced velocity by dividing with the square of the external field. Another important influence determining the fluid velocity is the height of the channel: it turns out that the velocity is larger in bigger channels. This leads us to reduce the velocity also by dividing by the height L of the duct. In order to get a dimensionless number, one also has to scale with the viscosity of the fluid. Thus we define

$$u = v_{\max} \frac{\eta}{L \mu_0 G_0^2} \tag{1}$$

as a reduced flow velocity. Its measured values are presented as a function of the driving frequency of the rotating magnetic field in figure 5. The measurements with each sample show a maximum of this velocity in the range of 30–40 kHz and 2–4 kHz, respectively.

4. Calculation of the fluid velocity

The pumping action can be understood as a manifestation of the magnetic stress acting on the magnetized fluid, as summarized in [10]. This assumption explains all qualitative features of the observation: as long as the magnetization is proportional to the magnetic field (which has been measured to be the case for our fluid, within a precision of 5% for fields up to about 1500 A m^{-1}), the stress must be proportional to G^2 as demonstrated in figure 4. If the frequency approaches zero, the magnetization and the field are parallel to each other, the tangential stress is zero and thus the motion of the fluid stops. For finite frequencies, the velocity is proportional to the χ'' component of the susceptibility, which must increase linearly (to lowest order) with the frequency. For higher frequencies, the imaginary part of the susceptibility χ'' has a maximum at a fluid-specific frequency, which explains that the maximal pumping velocity is observed around that frequency.

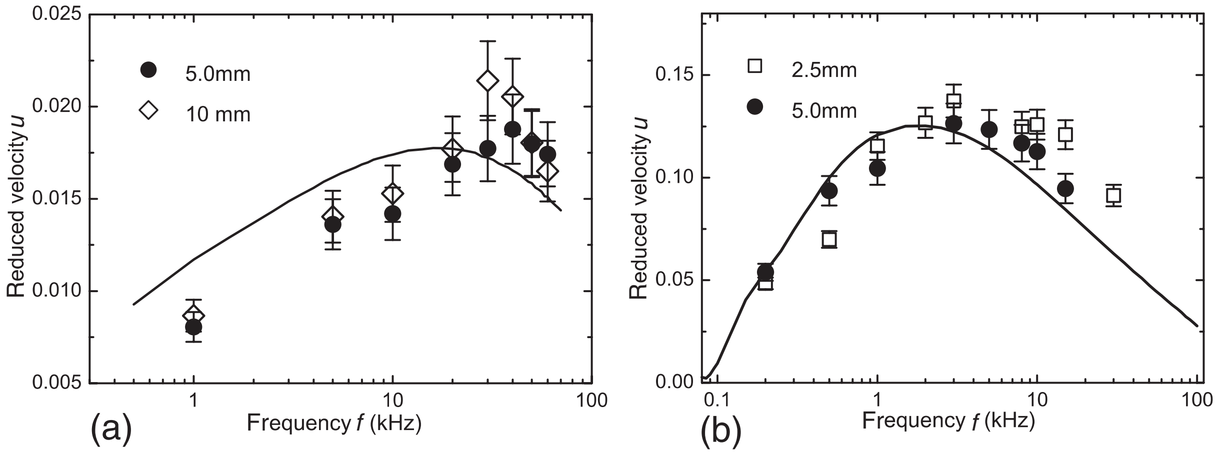

Figure 5. The reduced velocity u as a function of the driving frequency. For the magnetite fluid (a) solid circles (open diamonds) are obtained in the $5\,\text{mm} \times 5\,\text{mm}$ ($10\,\text{mm} \times 10\,\text{mm}$) duct, respectively; for the cobalt fluid (b) solid circles (open squares) are obtained in the $5\,\text{mm} \times 5\,\text{mm}$ ($2.5\,\text{mm} \times 2.5\,\text{mm}$) duct, respectively. The solid lines represent the values expected on the basis of the measurements of the ac-susceptibilities.

For the quantitative numerical calculation of the fluid velocity, we neglect the curvature of the duct. In this case, one can assume a primary flow with only an azimuthal x-component of the fluid velocity $v(y, z)$, where y corresponds to the radial and z corresponds to the vertical coordinate. The velocity field must fulfil the equation

$$\frac{\partial^2 v}{\partial y^2} + \frac{\partial^2 v}{\partial z^2} = 0.$$

The no-slip condition for the fluid at the bottom and the side walls of the duct then reads $v(y, 0) = v(0, z) = v(L, z) = 0$, where L measures both the width and the height of the square cross-section of the duct. The magnetic stress provides the boundary condition

$$\eta \frac{\partial v}{\partial z} = \frac{\mu_0}{2} |\boldsymbol{M} \times \boldsymbol{H}| \tag{2}$$

at the upper surface of the fluid, because equation (65) of [10] is applicable to our geometry. The two fields $\boldsymbol{H}$ and the corresponding magnetization $\boldsymbol{M}$ are not constant in our case, but depend both on time and space. In the following, we will first discuss the time dependence of the magnetic stress and then the spatial variation of the azimuthal and vertical components of the magnetic fields.

To describe the *time dependence* of the magnetic field and the magnetization of the fluid, we follow the procedure and nomenclature of [21]. An externally rotating magnetizing force $\boldsymbol{G} = \mathrm{Re}\{\hat{G}\}$, where

$$\hat{G} = \mathrm{e}^{\mathrm{i}\omega t}(G_\varphi, 0, -\mathrm{i}G_z),$$

leads to an elliptically rotating internal field $\boldsymbol{H} = \mathrm{Re}\{\hat{H}\}$ with

$$\hat{H} = \mathrm{e}^{\mathrm{i}\omega t}\left(G_\varphi, 0, \frac{-\mathrm{i}G_z}{1+N\chi}\right),$$

where the existence of an demagnetization factor N is assumed along the vertical direction. The corresponding inhomogeneity of the field also leads to field components in the radial direction, but these do not contribute to a stress in the azimuthal direction. The magnetic field produces a magnetization $\boldsymbol{M} = \mathrm{Re}\{\hat{M}\}$, where

$$\hat{M} = \mathrm{e}^{\mathrm{i}\omega t}\left(\chi G_\varphi, 0, \frac{-\mathrm{i}\chi G_z}{1+N\chi}\right).$$

The cross product in equation (2) can then be written as

$$|\boldsymbol{M}\times\boldsymbol{H}| = \tfrac{1}{4}|(\hat{M}+\hat{M}^*)\times(\hat{H}+\hat{H}^*)| = \tfrac{1}{4}|\hat{M}\times\hat{H}+\hat{M}\times\hat{H}^*+\hat{M}^*\times\hat{H}+\hat{M}^*\times\hat{H}^*|. \quad (3)$$

Inserting the azimuthal and vertical components of the field and magnetization into equation (3), the first and last time-dependent terms add up to zero each and only the time-independent terms remain:

$$|\boldsymbol{M}\times\boldsymbol{H}| = \left|\frac{-\mathrm{i}G_\varphi G_z}{4}\left(\frac{\chi}{1+N\chi}+\frac{\chi}{(1+N\chi)^*}-\frac{\chi^*}{(1+N\chi)^*}-\frac{\chi^*}{1+N\chi}\right)\right|.$$

Using the complex susceptibility $\chi = \chi' - \mathrm{i}\chi''$, one gets

$$|\boldsymbol{M}\times\boldsymbol{H}| = \left|\frac{-\mathrm{i}G_\varphi G_z}{4}\frac{(\chi-\chi^*)[(1+N\chi)+(1+N\chi)^*]}{|1+N\chi|^2}\right| = \frac{G_\varphi G_z(1+N\chi')\chi''}{|1+N\chi|^2}. \quad (4)$$

Putting the result of equation (4) into equation (2) we finally obtain

$$\eta\frac{\partial v}{\partial z} = \frac{\mu_0}{2}\frac{\chi''(1+N\chi')G_\varphi G_z}{(1+N\chi')^2+(N\chi'')^2}. \quad (5)$$

While both the magnetic field and the magnetization are rotating, the magnetic stress turns out to be time independent.

The *azimuthal component* of the magnetic field can be estimated on the basis of Ampere's law as

$$H_x(y) = G_\varphi\frac{d}{2(y+R_\mathrm{i})},$$

where d is the mean diameter of the duct and R_i its inner radius. While this equation is exact for a very large winding number of the coil, it is only approximately correct for our coil consisting of 50 windings. A relatively small number like this is necessary to allow an observation of the fluid flow. The difference can be checked by calculating the azimuthal magnetic field numerically using Biot–Savart's law. These calculations show a tiny x-dependence of the magnetic field due to the finite number of windings, but this deviation from the simplified assumption turned out to be smaller than 1% for every position along the surface of the duct.

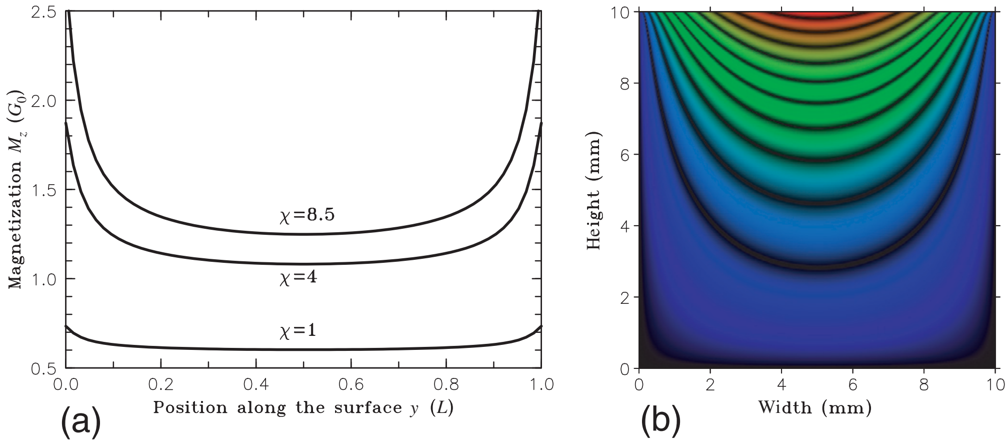

Figure 6. (a) The numerically obtained vertical component of the magnetization as a function of the radial position at the surface of the duct. Susceptibilities of $\chi = 1, 4$ and 8.5 have been used. (b) Numerical calculation of the velocity profile in the duct.

The *vertical component* of the magnetic field is slightly more complicated. While it would be almost perfectly homogenous on the surface of the empty duct, the magnetization of the fluid inside the duct gives rise to a radial dependence of H_z, which has to be obtained numerically for a given value of the magnetic susceptibility χ of the fluid inside the duct. To do so, we introduce the magnetic scalar potential ϕ_m with $\nabla\phi_m = \boldsymbol{H}$ and solve $\nabla^2\phi_m = 0$ by a relaxation method [22]. The magnetization is then calculated as $\boldsymbol{M} = \chi\boldsymbol{H}$. Figure 6(a) shows the result of this numerical calculation obtained for three different susceptibilities.

As a consequence of the magnetization shown in figure 6(a), and the radial dependence of the azimuthal component discussed above, the magnetic stress is not constant along the radial position on the surface. The corresponding boundary condition equation (5) can nevertheless be used for a numerical solution of the Laplace equation for the flow field. We get for the maximum fluid velocity in the middle of the upper surface

$$v_{\max} = \chi'' \frac{\mu_0 G_0^2}{2} \frac{L_z}{\eta} \beta(\chi, a). \tag{6}$$

Here the amplitudes G_φ and G_z have been set to the common value G_0. β is a factor which depends both on the susceptibility χ and the aspect ratio $a = L_y/L_z$ of the rectangular channel. In principle, we do not expect a simple analytical expression for β. To make the data examination practicable, however, we use an analytic expression which describes this factor with a precision of better than 1% within our range of interest ($0 < \chi < 10$), namely

$$\beta \approx \alpha \left(\frac{1 + N_{\text{eff}}\chi'}{(1 + N_{\text{eff}}\chi')^2 + (N_{\text{eff}}\chi'')^2} \right). \tag{7}$$

The two constants α and N_{eff} need some additional explanation.

The constant α must be introduced with respect to the finite geometry of the duct and can be obtained analytically for the limiting case $\chi \to 0$. In this case, the magnetization is uniform along

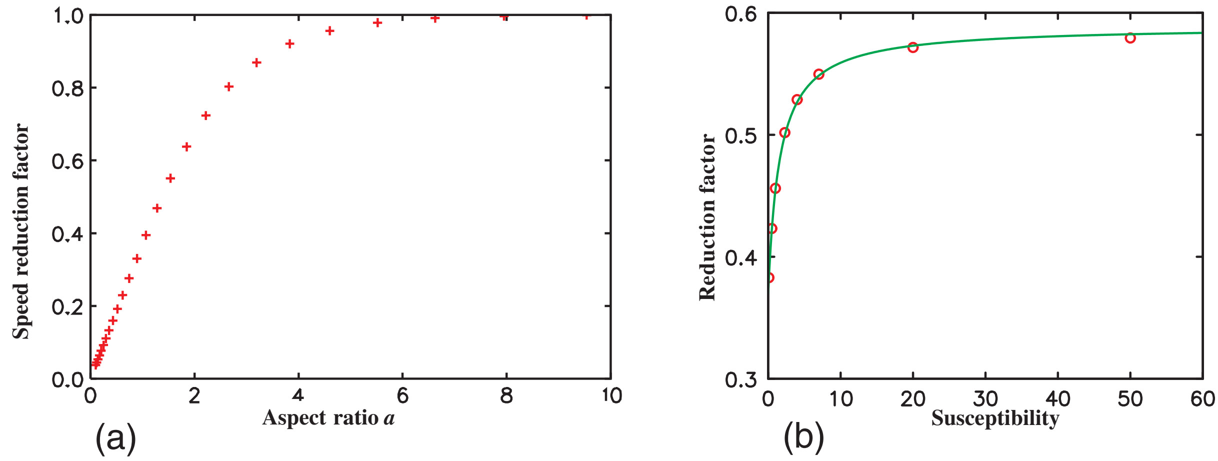

Figure 7. (a) The geometry factor α as function of different values of the aspect ratio a. (b) The numerically obtained speed reduction factor β for values of χ between 0 and 50. The green line shows the best fit using equation (7) with $\alpha = 0.369$ (applicable for our aspect ratio).

the radial position of the surface. The Laplace equation $\nabla^2 v = 0$ with the boundary conditions $v(y,0) = v(0,z) = v(L_y, z) = 0$ and the uniform magnetic stress $(\partial v(y, L_z))/(\partial z) = \mu_0 G_0^2/2\eta$ is solved by

$$v(y,z) = \frac{L_z \mu_0 G_0^2}{2\eta} 4a \sum_{n=1,3,5,..}^{\infty} \frac{\sin(n\pi y/L_z a)}{(n\pi)^2} \frac{\sinh(n\pi z/L_z a)}{\cosh(n\pi/a)}. \qquad (8)$$

Equation (8) follows for the maximal velocity as

$$v_{\max} = v(L_y/2, L_z) = \frac{L_z \mu_0 G_0^2}{2\eta} \sum_{n=1}^{\infty} (-1)^{n-1} \left(\frac{2}{\pi(2n-1)}\right)^2 \frac{a}{\sqrt{2}} \tanh\left(\frac{(2n-1)\pi}{a}\right). \qquad (9)$$

The speed reduction factor α results now from equation (9) via

$$\alpha = v_{\max} \frac{2\eta}{L_z \mu_0 G_0^2}$$

and depends only on the aspect ratio a. In our case of a quadratic-shaped duct ($a = 1$), we get a value of about 0.369 for α, as shown in figure 7(a). The case of an infinitely extended layer is included as

$$\lim_{a\to\infty} \alpha = 1.$$

The χ-dependence of the parameter β is only approximately captured by the ansatz of equation (7). This equation would only be correct for a homogenous magnetization of the fluid, which would be described by some demagnetization factor N. In the case of our square cross-section, the magnetization—and the ensuing stress at the surface of the fluid—is not homogenous, as demonstrated in figure 6(b). We thus extract an effective demagnetization factor N_{eff} by fitting equation (6) to the numerically obtained velocity for different values of χ. The results for β and the fit are displayed in figure 7(b). We obtain $N_{\mathrm{eff}} \approx 0.656$, which seems realistic when compared to $N = 0.5$ for the case of a circular cylinder.

From equations (1), (6) and (7) we finally get the theoretical estimation for the reduced velocity

$$u = \frac{\alpha}{2} \frac{\chi''(1 + N_{\mathrm{eff}}\chi')}{(1 + N_{\mathrm{eff}}\chi')^2 + (N_{\mathrm{eff}}\chi'')^2}. \tag{10}$$

The limiting case of an infinitely wide channel ($N = 1, \alpha = 1$) is included in this formula. The reduced velocity obtained from equation (10) is presented in figure 5 as a solid line, with the values of χ' and χ'' taken from the measurements presented in figure 2.

5. Discussion and conclusion

As the main result, the frequency dependence of the measured fluid velocity is reproduced by the calculations for both fluids over more than two decades. Inspecting figure 5 more carefully, we find that the agreement is less convincing in figure 5(a) than in figure 5(b), where an agreement on a 20% level can be found. The less convincing results for the magnetite-based fluid can be partly attributed to the much smaller imaginary part of the susceptibility, which aggravates a precise measurement of susceptibility and fluid velocity. Indeed, at the maximum of the imaginary susceptibility, the ratio χ''/χ' is about ten times smaller for the magnetite-based fluid, when compared to the one for cobalt-based fluid.

Statistical errors in both graphs stem from the limited accuracy of the measurement procedure of the fluid velocity, which is indicated by the error bars in figure 5. The systematic deviations between the data and the theoretical curve are believed to reflect the precision of the simplifying assumptions going into the consideration presented above. In particular, the radial component of the flow due to the finite channel diameter was not taken into account. Moreover, we have neglected an inhomogeneous temperature distribution due to energy dissipation within the magnetic fluid. It has been discussed in [23] that a spatial inhomogeneity of the temperature gives rise to a inhomogeneity of the magnetization. In this way an internal heating may slightly modify the magnetization calculated for the duct (figure 6).

In contrast to the geometry of [5], the influence of the shape of the meniscus of the fluid is comparatively small. We have minimized this influence furthermore by a brimful filling of the channel. Despite that, any meniscus is adding a three-dimensional complication to the problem, which has not been taken into account. Moreover, it should be noted that magnetic fluids are not perfectly stable both in their magnetic susceptibility and their viscosity, which might add to the small mismatch between the expectation based on the measurement of the susceptibility and the measured velocity. Finally, taking into account the small amplitude of the magnetic field, any magneto viscous effects have been neglected for the calculations.

To conclude, the pump presented here works well and has an interesting potential especially in micro- and nano-fluidic applications, where a mechanical driving of the flow is not possible.

More importantly, it does seem safe to conclude that the ansatz of a magnetic stress-driven motion captures the essence of this pump on a quantitative level.

Acknowledgments

It is a pleasure to thank A Engel and M I Shliomis for clarifying discussions. We thank M Krekhova for synthesizing the magnetite-based liquid, N Matoussevitch for providing the cobalt-based liquid and M Horn for measuring the viscosity of the samples. The experiments were supported by Deutsche Forschungsgemeinschaft, Re 588/12.

References

[1] Rosensweig R E 1985 *Ferrohydrodynamics* (Cambridge: Cambridge University Press)
[2] McTague J P 1969 *J. Chem. Phys.* **51** 133
[3] Bacri J-C, Perzynski R, Shliomis M I and Burde G 1995 *Phys. Rev. Lett.* **75** 2128
[4] Zeuner A, Richter R and Rehberg I 1998 *Phys. Rev.* E **58** 6287
[5] Moskowitz R and Rosensweig R 1967 *Appl. Phys. Lett.* **11** 301
[6] Brown R and Horsnell T S 1969 *Electron. Rev.* **14** 235
[7] Rosensweig R E, Popplewell J and Johnston R J 1990 *J. Magn. Magn. Mater.* **85** 171
[8] Shliomis M I 1974 *Sov. Phys.—Usp.* **17** 153
[9] Shliomis M I, Lyubimova T P and Lyubimov D V 1988 *Chem. Eng. Commun.* **67** 275
[10] Shliomis M I 2003 *Ferrofluids: Magnetically Controllable Fluids and Their Applications (Lecture Notes in Physics* vol 594) ed S Odenbach (Berlin: Springer) p 85
[11] Cebers A O 1975 *Magn. Gidrodinamika* **1** 79
[12] Cebers A O 1978 *Magn. Gidrodinamika* **4** 9
[13] Blums E, Cebers A and Maiorov M M 1997 *Magnetic Fluids* (Berlin: de Gruyter)
[14] Pshenichnikov A F and Lebedev A V 2000 Internal rotations in magnetic fluids *Magnetohydrodynamics* vol 36, ed M I Shliomis and A Cebers (Riga: Institute of Physics, University of Latvia) pp 317–26
[15] Liu M 2000 German Patent DE000019842848A1
[16] Liu M 1995 *Phys. Rev. Lett.* **74** 4535
[17] Bönnemann H, Brijoux W, Brinkmann R, Matoussevitch N, Waldöfner N, Palina N and Modrow H 2003 *Inorganica Chim. Acta* **350** 617
[18] Bönnemann H, Brijoux W, Brinkmann R, Matoussevitch N and Waldöfner N 2003 German patent DE 10227779.6
[19] Maiorov M M 1979 *Magnetohydrodynamics* **15** 135 (Translation)
[20] Krauss R, Liu M, Reimann B, Richter R and Rehberg I 2005 *Appl. Phys. Lett.* **86** 024102
[21] Lebedev A V, Engel A, Morozov K I and Bauke H 2003 *New J. Phys.* **5** 57
[22] Jackson J D 1998 *Classical Electrodynamics* (New York: Wiley)
[23] Pshenichnikov A F, Lebedev A V and Shliomis M I 2000 Internal rotations in magnetic fluids *Magnetohydrodynamics* vol 36, ed M I Shliomis and A Cebers (Riga: Institute of Physics, University of Latvia) pp 339–46